A kurtosis-based statistical measure for two-dimensional processes and its application to image sharpness

Article · January 2003

CITATIONS
51

READS
943

4 authors, including:

András E Vladár
National Institute of Standards and Technology
198 PUBLICATIONS **2,934** CITATIONS

SEE PROFILE

Michael T. Postek
University of South Florida
237 PUBLICATIONS **3,848** CITATIONS

SEE PROFILE

A Kurtosis-based Statistical Measure for Two-dimensional Processes and Its Applications to Image Sharpness

Nien Fan Zhang, Andras E. Vladar, Michael T. Postek, Robert D. Larrabee
National Institute of Standards and Technology, Gaithersburg, MD 20899

KEY WORDS: Autocorrelation; Discrete Fourier transform; Periodograms; Scanning electron microscope; Stationary process.

1. Introduction

Fully automated or semiautomatic scanning electron microscopes (SEM) are now commonly used in semiconductor production and other forms of manufacturing. It is required that these automated instruments be routinely capable of 3 nanometer (nm) or better resolution below 1kV accelerating voltage for the measurement of nominally 70-150 nm size parts of integrated circuits. Testing and proving that the instrument is performing at this level for production on a day-by-day basis, however, has not been routinely employed. Once a human operator is no longer monitoring the instrument's performance and multiple instruments are concerned, an objective diagnostic procedure must be implemented to ensure data and measurement fidelity.

Digital images are composed of individual image points also called pixels. Any image taken in a SEM is the result of the sample and electron probe interaction. The sharpness concept described in Postek and Vladar (1998) is a practical approach to the evaluation of instrument resolution. A degradation of the sharpness of the image of a suitable test object can serve as an indicator of the need for maintenance. Postek and Vladar (1996) proposed a procedure based on the image sharpness and it has subsequently been refined into a user-friendly stand-alone analysis system (Vladar, Postek and Davidson (1998)). The procedure was based on the objective characterization of the spatial Fourier transform of the SEM images of a test object. It was observed that when an SEM image is visually sharper than a second image, the high spatial frequency components of the first image are larger than those of the second. The following is an illustrative example. Figure 1a shows the performance of a cold Field Emission SEM on a heavily gold-coated oxide test sample at low accelerating voltage. This micrograph was taken following a poorly implemented maintenance procedure. This image appears to be less sharp and lacks resolution compared to a similar micrograph (Figure 1c) taken when the same instrument was operating optimally. Figure 1a appears to be far less sharp than Figure 1c. Figure 1b and 1d shows the magnitude distributions of the two-dimensional Fourier transforms or periodograms at spatial Fourier frequencies for the images in Figure 1a and 1c, respectively. From these figures it is clear that for the sharper image in Figure 1c, and its cone in 1d, which represents the periodogram of the image, is wider than that of the image in Figure 1b.

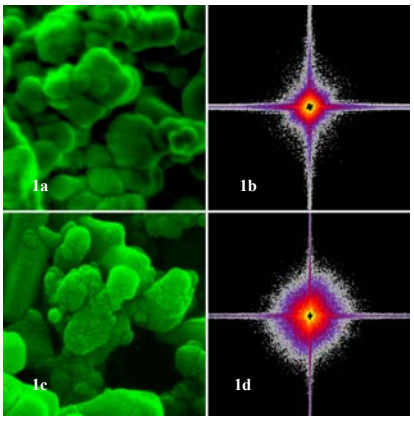

Figure 1. Two SEM Images and their 2-d periodograms

Recently, Batten (2000) investigated the use of sharpness search algorithms. Joy, Ko and Hwu (2001) proposed a method based on cross-correlation to provide an estimate of the signal to noise ratio of images.

The best performance of a SEM cannot be achieved unless pertinent parameters of the electron-optical column are correctly adjusted. Beyond the operator's skills and judgment, there are several methods that can be used to determine how well focus and astigmatism adjustments are set or to calculate the sharpness of an image compared to another one. These may work in the spatial or the Fourier domain and have different characteristics in terms of accuracy and noise tolerance. A statistical measure based on the bivariate kurtosis was proposed in Zhang, Postek, Larrabee, Vladar, Keery, and Jones (1997) and Zhang, Postek, Larrabee, Vladar, Keery, and Jones (1999) to measure the sharpness of the SEM images. In these papers, bivariate kurtosis as a function of moments up to the fourth of the distribution of a two-dimensional random vector has been used to measure the shoulder of the two-dimensional probability distribution. Treating the two-dimensional spectral density of a two-dimensional

stationary process as a probability density, this approach uses the bivariate kurtosis of the normalized periodograms of an SEM image to measure its sharpness. The kurtosis-based method described herein is one possible method among many. We do not yet undertake to compare the various methods Rather, the purpose of this paper is to (1) discuss the statistical issues of this approach in greater detail and provide some statistical basis for image sharpness measures and (2) demonstrate that the kurtosis-based method, which so far has been applied to image sharpness calculation only, can be extended to account for astigmatism. In Section 2, we will discuss the autocorrelation structures and the corresponding spectra for the two-dimensional stationary processes. In Section 3, we will discuss the multivariate kurtosis, especially, the bivariate kurtosis and its related properties. In Section 4, bivariate kurtosis is applied to the two-dimensional periodograms of SEM images to measure the image sharpness and a real example is presented, followed by the conclusions in Section 5.

2. Two-dimensional Stationary Processes

We consider a continuous two-dimensional stochastic process $\{X_{t,\tau}\}$, where $-\infty < t, \tau < \infty$. The process $\{X_{t,\tau}\}$ is called weakly stationary if

(1) $E[X_{t,\tau}] = \mu_x$, a constant for all t and τ

(2) $Var[X_{t,\tau}] = \sigma_x^2$, a constant for all t and τ

(3) The (two-dimensional) autocovariance function $Cov[X_{t,\tau}, X_{t+s,\tau+u}]$ only depends on s and u and is thus denoted by $R(s,u)$.

The indices t and τ can be for time and one-dimensional location or for two spatial parameters. We assume that all the processes are real-valued. For example a two-dimensional image process is a two-dimensional process formed by the image points with t and τ as the two spatial coordinates.

Similar to the one-dimensional case, $R(s,u) = R(-s,-u)$ for all s and u. Obviously, $\sigma_x^2 = R(0,0)$. The two-dimensional autocorrelation is defined as

$$\rho(s,u) = \frac{R(s,u)}{\sigma_x^2}$$

Similar to the one-dimensional case (e.g., see Priestley (1981), p. 720), the two-dimensional power spectral density function $f(\omega,\nu)$ is given by

$$f(\omega,\nu) = \left(\frac{1}{2\pi}\right)^2 \int_{-\infty}^{\infty}\int_{-\infty}^{\infty} \rho(s,u) e^{-is\omega - iu\nu}\, ds du$$

for $-\infty < \omega, \nu < \infty$. The function $f(\omega,\nu)$ exists for all ω and ν if

$$\int_{-\infty}^{\infty}\int_{-\infty}^{\infty} |\rho(s,u)|\, ds du < \infty$$

Obviously, $f(-\omega,-\nu) = f(\omega,\nu)$. Similar to the one-dimensional case (see Priestley (1981), p. 217), the spectral density function $f(\omega,\nu)$ has the following properties:

1. $\int_{-\infty}^{\infty}\int_{-\infty}^{\infty} f(\omega,\nu)\, d\omega d\nu = 1$
2. $f(\omega,\nu) \geq 0$
3. $f(-\omega,-\nu) = f(\omega,\nu)$ for all ω and ν.

Based on the properties in 1 and 2, the spectral density function $f(\omega,\nu)$ is like a two-dimensional probability density function of a bivariate random vector. Obviously, the normalized integrated spectrum

$$F(\omega,\nu) = \int_{-\infty}^{\omega}\int_{-\infty}^{\nu} f(\xi,\psi)\, d\xi d\psi$$

is like a bivariate cumulative probability distribution function.

3. Multivariate Kurtosis

For a univariate random variable Z with mean μ_z and finite moments up to the fourth, the kurtosis is defined as

$$\beta_2 = \frac{E[(Z-\mu_z)^4]}{\{E[(Z-\mu_z)^2]\}^2}$$

Assuming the probability density function $f_z(x)$ ($-\infty < x < \infty$) exists, the k^{th} central moment is

$$m_k = E[(Z-\mu_z)^k] = \int_{-\infty}^{\infty} (x-\mu_z)^k f_z(x)\, dx$$

Thus,

$$\beta_2 = \frac{m_4}{(m_2)^2} \qquad (1)$$

It is well known that for any univariate random variable with a Gaussian distribution, $\beta_2 = 3$. The

value of β_2 of a random variable can be compared with 3 to determine whether its distribution is "peaked" or "flatted-topped" relative to a Gaussian distribution. Four separate density functions with zero mean and unit variance were compared by Kapansky (1945) to illustrate this property of kurtosis. His results show that the smaller the kurtosis, the flatter the top of the distribution. Finucan (1964) also discussed the interpretations of kurtosis. Figure 2 shows the probability density functions of the standard Gaussian distribution (solid line), the density $R(x)$ (dashed line) and the density function $S(x)$ (dotted line) both discussed in Kaplansky (1945). All of these three distributions have unit variance. The distribution with the density of $R(x)$ has a kurtosis of 4.5. The distribution with the density function of $S(x)$ has a kurtosis of 2.667. It is clear that the distribution with a smaller kurtosis is more flat-topped or has a larger shoulder than that with a larger kurtosis. The distribution with the density function of $S(x)$ proposed by Kaplansky (1945) with $\beta_2 = 2.667$ has the largest shoulder among the three distributions.

Multivariate kurtosis has been proposed by Mardia (1970). Let W be a p-dimensional random vector with finite moments up to the fourth. Let μ_w be the

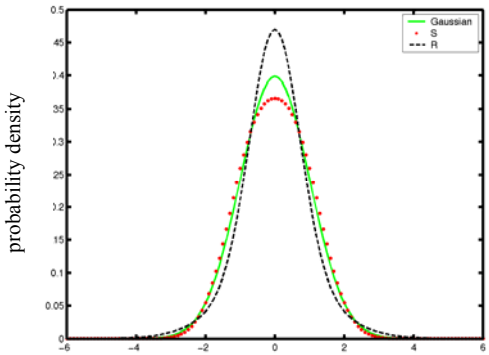

Figure 2. Probability density functions of three distributions

mean vector and Σ be the covariance matrix of W. The kurtosis of W is defined as

$$\beta_{2,p} = E\{(W-\mu_w)'\Sigma^{-1}(W-\mu_w)\}^2 \qquad (2)$$

When $p=1$, $\beta_{2,1}$ becomes the univariate kurtosis, β_2, in (1). From Mardia (1970) the bivariate kurtosis for $W=(W_1,W_2)'$ is calculated by

$$\beta_{2,2} = \frac{\gamma_{4,0}+\gamma_{0,4}+2\gamma_{2,2}+4\rho_{12}(\rho_{12}\gamma_{2,2}-\gamma_{1,3}-\gamma_{3,1})}{(1-\rho_{12}^2)^2} \qquad (3)$$

where ρ_{12} is the correlation between W_1 and W_2 and $\gamma_{k,l}$ for $k,l = 0,1,2,3,4$, is calculated by

$$\gamma_{k,l} = \frac{E[(W_1-\mu_1)^k(W_2-\mu_2)^l]}{\sigma_1^k\sigma_2^l} \qquad (4)$$

and μ_1,μ_2,σ_1, and σ_2 are the marginal means and marginal standard deviations of W_1 and W_2, respectively. In particular, when W is a bivariate Gaussian random vector, the corresponding bivariate kurtosis $\beta_{2,2}$ = 8. Figure 3 shows the probability density function of a standardized bivariate Gaussian random vector with ρ_{12} = 0.5. In Figure 4, a probability density function of a bivariate central t distribution with a degree of freedom of 9 was generated based on Equation 1 in Johnson and Kotz (1972), p. 134. The bivariat t distribution is the joint distribution of $W_i = X_i\sqrt{\nu}/S$ ($i=1,2$), where X_1 and X_2 have a joint standardized bivariate Gaussian distribution with correlation of X_1 and X_2 equal to ρ_{12}. The ρ_{12} in the bivariate t distribution in Figure 4 equals 0.5 The random variable S in the definition of W_i is independent of X_i ($i=1,2$) and is distributed

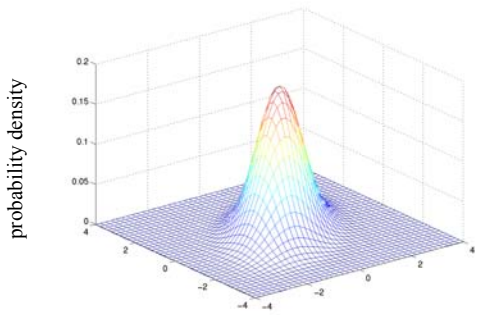

Figure 3. Probability density function of 2-d Gaussian distribution

as χ_ν with a degree of freedom of ν. The product moments of W_1 and W_2 are calculated and expressed by Gamma functions as follows:

$$E[W_1^kW_2^l] = \nu^{\frac{k+l}{2}}E[X_1^kX_2^l]E[\chi_\nu^{-(k+l)}]$$
$$= \left(\frac{\nu}{2}\right)^{\frac{K+l}{2}}E[X_1^kX_2^l]\frac{\Gamma\left(\frac{\nu-k-l}{2}\right)}{\Gamma\left(\frac{\nu}{2}\right)}$$

provided $k+l<\nu$. The second equality holds because

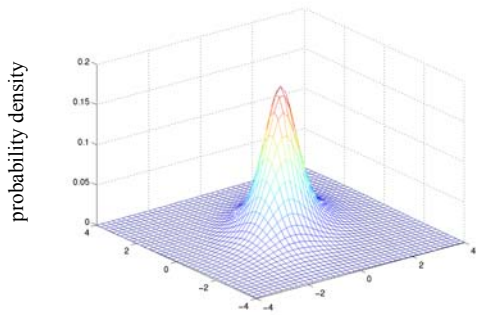

Figure 4. Probability density function of a 2-d t distribution

$$E[\chi_\nu^{-(k+l)}]=\left(\frac{1}{2}\right)^{\frac{k+l}{2}}\frac{\Gamma\left(\frac{\nu-k-l}{2}\right)}{\Gamma\left(\frac{\nu}{2}\right)}$$

The moment $E[X_1^k X_2^l]$ (k,l = 0,1,2,3,4 and $k+l<4$) can be obtained from Patel and Read (1982), p. 309. The correlation between W_1 and W_2 is also ρ_{12}. The kurtosis of the bivariate t distribution, $\beta_{2,2}$, can be obtained from (3). It is easy to show that for a bivariate t distribution, when $\nu>4$, $\beta_{2,2}$ is independent of ρ_{12} and only depends on ν. In fact,

$$\beta_{2,2}=8\frac{\Gamma\left(\frac{\nu-4}{2}\right)\Gamma\left(\frac{\nu}{2}\right)}{\left\{\Gamma\left(\frac{\nu-2}{2}\right)\right\}^2}$$

In this case the kurtosis of the bivariate t distribution with a degree of freedom of 9 is $\beta_{2,2}$=11.2. Figures 3 and 4 show that the curvature for the two-dimensional Gaussian distribution with a smaller bivariate kurtosis (=8) has a larger shoulder than that for the bivariate t distribution with a degree of freedom of 9, which has a larger bivariate kurtosis (=11.2).

For the marginal distributions of a bivariate random vector $W=(W_1,W_2)'$, the corresponding marginal kurtoses, denoted by β_{2,w_1} and β_{2,w_2} are the univariate kurtoses for W_1 and W_2, respectively. In fact, from (4) and (1),

$$\beta_{2,w_1}=\gamma_{4,0} \text{ and } \beta_{2,w_2}=\gamma_{0,4} \qquad (5)$$

Since marginal kurtoses can be used to measure the shapes of the shoulders of the corresponding marginal distributions, they are used in detecting the astigmatism and instrument vibrations. We will discuss this application in next section.

4. Bivariate Kurtosis to Measure Image Sharpness

As mentioned in Section 2, a two-dimensional spectral density is like a probability density function. In Section 3, we have shown that the bivariate kurtosis is a measure of the shoulder of a two-dimensional probability density function. Thus, treating a two-dimensional spectral density as a probability density function, the corresponding bivariate kurtosis is a measure of the shape of the shoulder of the two-dimensional spectral density.

For a two-dimensional stationary process, the spectral density $f(\omega,\nu)$ is usually estimated by its two-dimensional discrete realizations. For a given set of discrete two-dimensional lattice data, $\{w_{t,\tau};t,\tau=1,2,...,N\}$ the two-dimensional discrete Fourier transform is

$$\xi(\omega,\nu)=\frac{1}{2\pi N}\sum_{t=1}^{N}\sum_{\tau=1}^{N}w_{t,\tau}e^{-it\omega-i\tau\nu}$$

for $\omega,\nu=2\pi\lambda/N;-[(N-1)/2]\le\lambda\le[N/2]$, where [x] denotes the largest integer not exceeding x. The corresponding two-dimensional periodogram (see, Koopmans (1974), p. 258 and Preiestley (1981), p. 722),

$$I(\omega,\nu)=|\xi(\omega,\nu)|^2=\frac{1}{(2\pi N)^2}\left|\sum_{t=1}^{N}\sum_{t=1}^{N}w_{t,\tau}e^{-it\omega-i\tau\nu}\right|^2 \qquad (6)$$

is an estimator of the two-dimensional spectral density. It is well known that for any given ω and ν, the expectation of $I(\omega,\nu)$ approaches $f(\omega,\nu)$ when N goes to infinity (Priestley (1981), pp. 722-723). That is, $I(\omega,\nu)$ is an asymptotically unbiased estimator of the two-dimensional spectral density. The frequencies for $\omega,\nu=2\pi\lambda/N;-[(N-1)/2]\le\lambda\le[N/2]$ are called Fourier frequencies (e.g., see Ripley (1981), p. 80). The corresponding $\{I(\omega,\nu)\}$ are the values of periodogram at these Fourier frequencies. For simplicity denote these frequencies by $\omega_i,\nu_i(i=1,2,...,N)$.

For a discrete probability distribution, the bivariate kurtosis is calculated by the formulas in Section 3. A

discrete density based on $\{I(\omega_i, \nu_j)\}, i, j = 1, 2, ..., N$ is obtained by normalization. Namely,

$$h(\omega_i, \nu_j) = \frac{I(\omega_i, \nu_j)}{\sum_{m=1}^{N}\sum_{n=1}^{N} I(\omega_m, \nu_n)} \tag{7}$$

for $i, j = 1, 2, ..., N$. The corresponding marginal means and variances of $h(\omega, \nu)$ are calculated by

$$\mu_\omega = \sum_{i=1}^{N} \omega_i \sum_{j=1}^{N} h(\omega_i, \nu_j)$$

$$\mu_\nu = \sum_{j=1}^{N} \nu_j \sum_{i=1}^{N} h(\omega_i, \nu_j) \tag{8}$$

and

$$\sigma_\omega^2 = \sum_{i=1}^{N} (\omega_i - \mu_\omega)^2 \sum_{j=1}^{N} h(\omega_i, \nu_j)$$

$$\sigma_\nu^2 = \sum_{j=1}^{N} (\nu_j - \mu_\nu)^2 \sum_{i=1}^{N} h(\omega_i, \nu_j) \tag{9}$$

Then from (4) the corresponding $\gamma_{k,l}$ for $k, l = 0, 1, 2, 3, 4$ is

$$\gamma_{k,l} = \frac{\sum_{j=1}^{N}\sum_{i=1}^{N} h(\omega_i, \nu_j)(\omega_i - \mu_\omega)^k (\nu_j - \mu_\nu)^l}{\sigma_\omega^k \sigma_\nu^l} \tag{10}$$

The bivariate kurtosis corresponding to $\{h(\omega_i, \nu_j)\}$ can be obtained by (10). Therefore, for a given image, we have the corresponding bivariate kurtosis calculated based on the two-dimensional periodogram of the image.

When the beam of SEM scans the sample, the zero frequency component ($\omega, \nu = 0$) corresponds to the average gray level of the image. As we move away from the origin of the frequencies, the low frequencies correspond to the slowly varying components of an image or the large features. When we move further away from the origin, the higher frequencies begin to correspond to faster and faster gray level changes in the image, which gives data on finer details such as the edges. On the other hand, very high frequencies corresponding to abrupt changes in gray level compose the noise. See the discussions in Gonzalez and Woods (2001), pp. 156-157. An image of a sample, which has fine details at a given magnification, is sharper if there are more high frequency (but not too high) changes in it. Russ (1994), pp. 306-307, used an example to show that "The frequency transform of an image can be used to optimize focus and astigmatism. When an image is in focus, the high-frequency information is maximized in order to sharply define the edges. This provides a convenient test for sharpest focus." In that sense, kurtosis, which measures the width of the shoulder of the distribution corresponding to the strength at the high frequencies, but not too high, is used to measure image sharpness. This means that when the bivariate kurtosis of the (normalized) periodogram corresponding to one image is smaller than that for a second image, the first image is sharper than the second one. The example in the introduction shows the relationship between the image sharpness and the width of the bivariate periodogram. An SEM image is represented by a set of discrete two-dimensional lattice data. The corresponding two-dimensional periodogram with the zero frequency at the center is calculated from (6). From the discussion in Section 3, between two SEM images, a sharper image which corresponds to a smaller bivariate kurtosis of the periodogram has a larger shoulder or has a flatter shape.

From (10), the marginal kurtoses of the marginal distributions of ω and ν are $\beta_{2,\omega} = \gamma_{4,0}$ and $\beta_{2,\nu} = \gamma_{0,4}$. The marginal kurtoses are used to measure the shapes of the shoulders of the marginal distributions. The difference between the marginal kurtoses measures the difference between the widths of the shoulders of the marginal distributions. When astigmatism is present, the two-dimensional power spectrum is asymmetric (see, e.g., Russ (1994), pp. 306-307). Th marginal kurtoses can be used to detect the asymmetry of the periodogram in vertical and horizontal sections corresponding to the astigmatism or misalignment in the image caused by possible instrument vibration. We use

$$\frac{\left|\beta_{2,\omega} - \beta_{2,\nu}\right|}{\min(\beta_{2,\omega}, \beta_{2,\nu})} \tag{11}$$

to measure the relative difference of the marginal kurtoses.

The following example demonstrates how the bivariate kurtosis is used to measure the sharpness of SEM images. The sample is an etched silicon wafer with the artifact referred to as "grass", an etching artifact that can occur on silicon wafers during processing, as stated in Postek (1994). In Figure 5, a series of five micrographs shows a representative set of experiments developed to demonstrate the sharpness analysis procedure. All the micrographs were taken by the same instrument with only one parameter changed for each image. Figure 5a is a micrograph of the grass sample

taken with the SEM conditions set for focus images. Figure 5b is a similar micrograph also under focus condition. Figure 5c is a micrograph, which is not properly focused. Figure 5d is a micrograph with astigmatism in the horizontal direction. Figure 5e is a micrograph also with astigmatism but in the vertical direction.

The second row in Figure 5 shows the magnitude distributions of the two-dimensional periodograms corresponding to the images in Figure 5a – 5e. Darker points mean high magnitudes of the values of a periodogram. Each two-dimensional periodogram is calculated based on 1024 by 1024 Fourier frequency points. The third row in Figure 5 shows the same magnitude distributions as in the second row after some image processing (and coloring) to show the inner structure of the two-dimensional periodograms better.

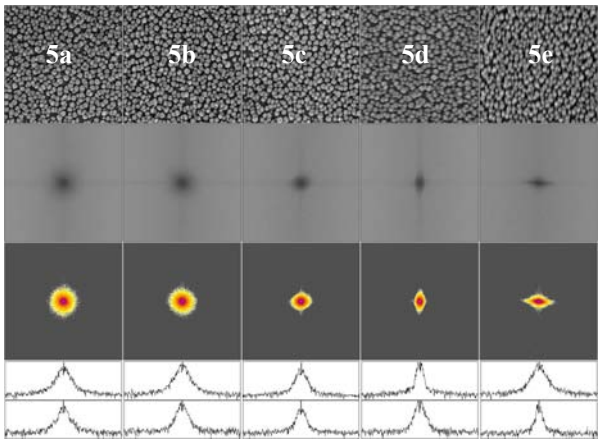

Figure 5. Five micrographs and their 2-d and 1-d periodograms

The fourth and the last rows show the one-dimensional periodograms corresponding to the horizontal and vertical directions for the images in Figure 5a-5e, respectively.

Bivariate kurtosis of the two-dimensional periodograms were calculated by (5) – (10) and (3) for the micrographs. Figure 6 is the graphical representation of kurtoses. As discussed earlier, a low number for kurtosis indicates a better quality image or high sharpness. Micrographs in Figure 5a (focused) and 5b (2nd focused) are the known good images with kurtosis values of 5.90 (for Figure 5a) and 5.93 (for

Marginal kurtosis can be used to measure whether an image contains astigmatism. We found that when astigmatism does exist, the relative difference between the marginal kurtoses corresponding to the horizontal and vertical profiles of the two-dimensional periodogram and calculated by (5) and (11) will show

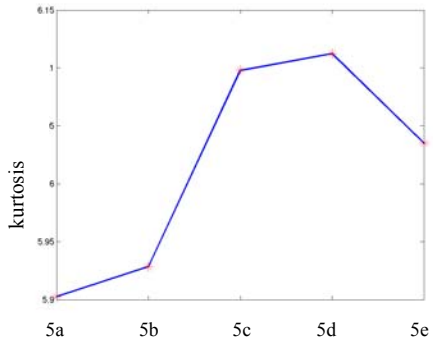

Figure 6. Bivariate kurtosis of 5 sample images

Figure 5b). The image in Figure 5a is slightly sharper than that in Figure 5b. The visually poorer image in Figure 5c (not focused) exhibits a higher kurtosis value of 6.10. The images with astigmatism in Figures 5d and 5e have higher kurtosis values, which indicate that they are not sharp. The kurtosis value for the micrograph in Figure 5e is lower than that in Figure 5c, the one not focused. Does this mean that the image in Figure 5e is sharper than that in Figure 5c? We will discuss this issue below. In calculating the two-dimensional kurtoses, very high frequencies are cut off since they are all noise.

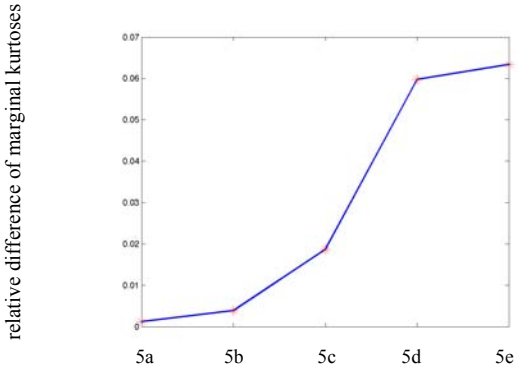

Figure 7. Relative difference of marginal kurtoses

high value than that which contains no astigmatism. Figure 7 shows the relative differences of marginal kurtoses. The images in Figures 5d and 5e demonstrate a much greater relative kurtosis difference (0.06) compared with the focused images (0.0012 and 0.0039) in Figures 5a and 5b and the one not focused (0.019) in Figure 5c. The anomalous data set becomes obvious when a study of the relative difference of marginal kurtoses is performed. The high relative difference of marginal kurtoses is an indicator that

something is radically wrong and a service measure should be implemented. Therefore, checking the marginal kurtosis difference would be the first cut to eliminate anomalous data such as those seen in Figures 5d and 5e.

Using bivariate kurtosis to measure the sharpness of a SEM image has an advantage because the dimensionless kurtosis is insensitive to scale factor of the image. See the detailed discussion in Postek, Vladar, Zhang, and Larrabee (2000). Based on bivariate kurtosis and other measures of image sharpness, in collaboration with NIST and Hewlett-Packard, the Spectel Co. developed the image-sharpness monitor and incorporated it into a software package running on a workstation system signifying the need for SEM performance monitoring. NIST now is offering an SEM image sharpness reference artifact (RM 8091), which can be used successfully for these procedures.

5. Conclusion

The kurtosis of a probability distribution has been used to measure the shape and width of the shoulder of the distribution. This property is exploited to the spectral density for a two-dimensional stationary process and then applied to SEM to measure image sharpness. The bivariate kurtosis and the corresponding relative difference of the marginal kurtoses are implemented in a workstation system and used in semi-conductor industry for SEM performance monitoring. In fact, this approach can apply to any image generating system including SEM to measure image sharpness. In a forthcoming paper we will compare the effectiveness of various sharpness measures.

6. References

Batten, C. F. (2000), "Autofocusing and Astigmatism Correction in the Scanning Electron Microscope," http://www.cag.lcs.mit.edu/~cbatten/batten-phil00.pdf.

Finucan, H. M. (1964), "A Note on Kurtosis," Journal of Royal Statistical Society, B, 26, 111-112.

Gonzalez, R. C. and Woods, R. E. (2001), Digital Image Processing, Prentice-Hall, Inc.

Johnson, N. L. and Kotz, S. (1972), Distributions in Statistics: Continuous Multivariate Distributions, Wiley, New York.

Johnson, N. L., Kotz, S., and Balakrishnan, N (1995), Continuous Univariate Distributions, Volume 2, 2nd edition, Wiley, New York.

Joy, D. C., Ko, Y., Hwu, J. (2001), http:/web.utk.edu/~srcutk/smartstuff/metrics.pdf.

Kapansky, I. (1945), "A Common Error Concerning Kurtosis," Journal of American Statistical Association, 40, 259.

Koopmans, L. H. (1974), The Spectral Analysis of Time series, Academic Press.

Mardia, K. V. (1970), "Measures of Multivariate Skewness and Kurtosis with Application," Biometrika, 57(3), 519 - 530.

Patel, J. K. and Read, C. B. (1982), Handbook of the Normal Distribution, Marcel Dekker, New York.

Postek, M. T. (1994), "Critical Issues in Scanning Electron Microscope Metrology," NIST Journal of Research, 99(5), 641-671.

Postek, M. T. and Vladar A. E. (1996), "SEM Sharpness Evaluation using Sharpness Criterion," Proc. SPIE, 2725, 504-514.

Postek, M. T. and Vladar A. E. (1998), "Image Sharpness Measurement in Scanning Electron Microscope – Part I," Scanning, 20, 1-9.

Postek, M. T., Vladar, A. E., Zhang, N. F., and Larrabee, R. D. (2000), "Potentials of On-line Scanning Electron Microscope Performance Analysis Using NIST Reference Material 8091," Proc. SPIE, 3998, 28-37.

Priestley, M. B. (1981), Spectral Analysis and Time Series, Academic Press, London.

Ripley, B. D. (1981), Spatial Statistics. Wiley, New York.

Russ, J. C. (1994), The Image Processing Handbook, 2nd edition, CRC Press.

Vladar, A. E., Postek, M. T., and Davidson, M. P. (1998), "Image sharpness measurement in scanning electron microscope – Part II", Scanning, 20, 24-34.

Zhang, N. F., Postek, M. T., Larrabee, R. D., Vladar, A. E., Keery, W. J., and Jones, S. N. (1997), "A Statistical Measure for the Sharpness of the SEM Images, Proc. SPIE, 3050, 375-387.

Zhang, N. F., Postek, M. T., Larrabee, R. D., Vladar, A. E., Keery, W. J., and Jones, S. N. (1999), "Image Sharpness Measurement in the Scanning Electron Microscope – Part III", Scanning, 21, 246-252.